Received: 11 November 2023 | Revised: 28 January 2024 | Accepted: 3 February 2024

DOI: 10.1002/mop.34082

RESEARCH ARTICLE

WILEY

Dynamically tuning and reconfiguring microwave bandpass filters using optical control of switching elements

Peizhao Li | **Ehsan Zahedi** | **Yu Shi** | **Yijing Deng** | **Lei Liu**

Department of Electrical Engineering, University of Notre Dame, Notre Dame, Indiana, USA

Correspondence
Lei Liu, Department of Electrical Engineering, University of Notre Dame, 275 Fitzpatrick Hall of Engineering, Notre Dame, IN 46556, USA.
Email: lliu3@nd.edu

Funding information
National Science Foundation, Grant/Award Numbers: 1711052, 1711631, 2223949

Abstract

We report a novel approach for dynamically tuning and reconfiguring microwave bandpass filters (BPFs) based on optically controlled switching elements using photoconductivity modulation in semiconductors. For a prototype demonstration, a BPF circuit featuring a second-order design using two closely coupled split-ring resonators embedded with multiple silicon chips (as switching elements) was designed, fabricated, and characterized. The silicon chips were optically linked to fiber-coupled laser diodes (808 nm light) for switching/modulation, enabling dynamic tuning and reconfiguring of the BPF without any complex biasing circuits. By turning on and off the two laser diodes simultaneously, the BPF response can be dynamically reconfigured between bandpass and broadband suppression. Moreover, the attenuation level of the passband can be continuously adjusted (from 0.7 to 22 dB at the center frequency of 3.03 GHz) by varying the light intensity from 0 to 40 W/cm^2. The tuning/reconfiguring 3-dB bandwidth is estimated to be ~200 kHz. In addition, the potential and limitations of the proposed approach using photoconductivity modulation are discussed. With the strong tuning/reconfiguring capability demonstrated and the great potential for high-frequency operation, this approach holds promise for the development of more advanced tunable filters and other adaptive circuits for next-generation sensing, imaging, and communication systems.

KEYWORDS

bandpass filter, optically controlled modulation, silicon

1 | INTRODUCTION

In typical modern adaptive communication systems, the implementation of tunable multiband bandpass filters (BPFs) is often desired for reconfigurable signal path due to the nature of a single transceiver operating across multiple frequency bands concurrently.[1] Dynamically switching among different frequency channels/bands is also important for effective usage of spectrum since some bands are either empty or not used at full capacities.[2] In addition, sensing the income signal spectrum information based on frequency control circuits (e.g., tunable BPFs) becomes more and more important for adapting the link parameters for operation in certain frequency bands.[3] To realize the above functionalities in modern systems, switched filter banks[4] comprising an array of tunable/reconfigurable BPFs as shown in Figure 1A can play a pivotal role. These BPF elements collectively serve to divide the input signal into multiple components, each singularly containing a distinct frequency sub-band derived from the original signal, offering the potential to greatly reduce system complexity and enable multifunctionality.[4]

As a consequence, a range of microwave tunable/reconfigurable BPFs and/or switched multiplexer topologies have been proposed and designed employing various switching technologies based on either semiconductor-based devices (e.g., field-effect transistors [FETs], PIN diodes, varactors)[5–7] or micro-electro-mechanical systems (MEMS) devices,[8] for achieving such filter banks. These filter banks demonstrated incorporate tuning/switching elements positioned either before multiple channels (switched multiplexer design) or within each filter inside a band (tunable BPF design).[5–8] However, all the aforementioned switching technologies require complex biasing circuitry for their operation. This unavoidably introduces performance challenges due to parasitic effects from the bias circuitry, while also posing difficulties in circuit design, integration, and fabrication. This situation becomes more severe as frequencies enter the millimeter-wave to THz (mmW-THz) region (with smaller circuit sizes) for next-generation (e.g., 6G and beyond) communication systems.[9] In addition, semiconductor-based switches typically exhibit significant performance degradation at mmW-THz,[10] making them unsuitable for future systems. Although MEMS switches can be applied (in the mmW-THz range), their extremely challenging fabrication, low speed, and potential reliability issues make them difficult to integrate into sophisticated and multifunctional systems.[10]

To address these challenges and develop an alternative approach for achieving high-performance multi-functional filter circuits required in next-generation communication systems, a novel optical switching technology based on the modulation of semiconductor photoconductivities has been introduced and explored.[11] This switching technology, previously validated in both D-band and G-band (110–220 GHz) using silicon,[12] has been successfully employed to demonstrate a versatile and adaptable bandstop filter (BSF) using split-ring resonators (SRRs)[13] in the absorption mode. To further unlock the technology potential, demonstrate the design flexibility, and attain dynamic tunability for various applications, in this paper, we propose and demonstrate a prototype single band tunable and reconfigurable BPF element (see channel 1 in Figure 1B) based on transmission-mode SRRs as an approach for achieving more complex switched filter banks as depicted in Figure 1. In pursuit of achieving a high roll-off filter response, a pair (second order) of identical transmission-mode SRRs were closely coupled (electric coupling structure[14]) to introduce distinct passbands. To enable reconfigurability and tunability, a micromachined silicon chip is embedded in the gap of each SRR. Each chip is optically linked to a fiber-coupled laser diode (808 nm)

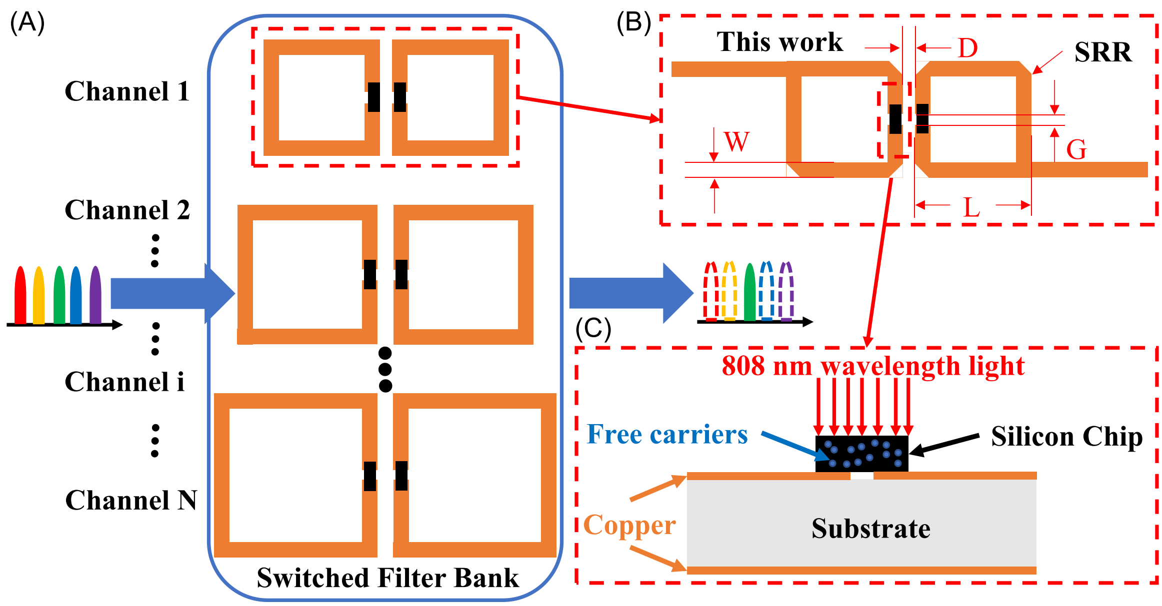

FIGURE 1 (A) The conceptual configuration of a switched multiband filter bank with a reconfigurable BPF for each band, (B) tunable and reconfigurable bandpass filters (BPFs) element for a prototype demonstration, and (C) the mechanism of photoconductivity modulation for RF switching using photo-induced free carriers in Si thin film. SRR, split-ring resonator.

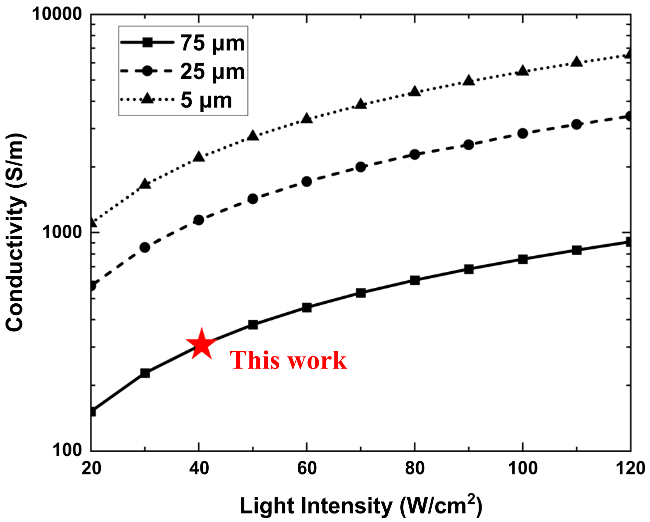

FIGURE 2 The photoconductivity of Si thin film (assume a carrier lifetime of 1 μs) as a function of light intensity for different Si film thickness.

for the control of photoconductivity. By changing the illumination light simultaneously from the two fiber-coupled laser diodes, the passband can be dynamically reconfigured (i.e., on or off) and continuously tuned. This approach eliminates the need for additional biasing circuits to achieve tuning and reconfiguring, thereby reducing circuit complexity and enhancing frequency scalability, particularly in the context of higher-order BPF designs at high frequencies. By using the combination of absorption-mode SRRs (for BSFs) and transmission-mode SRRs (for BPFs), a wide range of tunable/reconfigurable filters with various frequency responses (e.g., arbitrary frequency/bandwidth) and multiple functionalities can be achieved.

2 | THEORY FOR OPTICALLY CONTROLLED RF SWITCHING

As discussed above, the prototype BPF element (Figure 1B to be demonstrated in this paper consists of two closely coupled transmission-mode SRRs with embedded optical switching elements at their gaps. The dynamically tuning and reconfiguring of the BPF are achieved by exposing the switching elements (semiconductor layer, e.g., silicon) with light to control its photoconductivity. Upon absorption of a photon (with energy level larger than the bandgap of semiconductor), an electron situated within the valence band of the semiconductor gains the requisite energy for its transition to the conduction band.[11] This absorption event leads to the generation of free carriers, i.e. electrons and holes with a carrier concentration n partially modulated by the incident light intensity. These electrons and holes exhibit different rates of movement under the influence of an electric field, depending on their mobility μ_n (electrons) and μ_p (holes), within the material.[15] Meanwhile, recombination of electrons and holes occurs during this process, which in turn results in an effective carrier lifetime τ and hence an effective carrier concentration n.[13] Therefore, in addition to incident light intensity, both mobility and effective carrier lifetime significantly contribute to the material's conductivity σ as determined by the following equation:

$$\sigma = q(\mu_n + \mu_p)n, \tag{1}$$

where q is the elementary charge. For instance, using silicon as a reference (with specific parameters for the high-resistivity Si (HRS, $\rho = 20{,}000\,\Omega\cdot\text{cm}$) employed in this work), the calculation of photoconductivity can be conducted based on light intensity and film thickness using an established physics-based nonlinear model in Shi et al.[11] The results (using Si as an example), as depicted in Figure 2, show that with an increase in light intensity, photoconductivity initially exhibits nearly linear growth, but it gradually plateaus as it approaches the threshold of approximately 120 W/cm^2. This leveling off can be attributed to Auger recombination at high carrier concentrations.[11] In addition, thinner material shows a higher photoconductivity. These findings emphasize the potential to achieve significant alteration in conductivity, with a ratio (on and off) reaching approximately 10^5, indicating its potential for achieving high-performance switching for tuning and reconfiguring microwave circuits, especially BPFs.

It is worth to note that the transient analysis using the physics-based model reveals that semiconductors typically undergo a 10-fold carrier lifetime cycle τ to achieve their maximum carrier concentration and an additional 10τ for recovery.[16] Among three materials discussed in Kannegulla et al.,[16] as compared to Si, Ge offers the longest carrier lifetime and hence the highest achievable carrier concentration and photoconductivity, while having the lowest modulation speed. On the contrary, GaAs provides the highest modulation speed but generating significantly lower carrier concentration and photoconductivity. In this paper, Si has been chosen for a proof-of-concept demonstration for dynamically tuning and reconfiguring a microwave BPF as shown in Figure 1. The effective carrier lifetime for the Si employed is estimated to be ~1 μs based on our previous experiment in Cheng et al.,[17] Ren et al.,[18] Jiang et al.,[19] and the diffusion length of ~41.6 μm is calculated. This selection aligns with the aim of achieving a balance between tuning speed and achievable conductivity (and corresponding switch RF performance) to fulfill the specific requirements (e.g., dynamic tuning with high modulation speed) of certain applications.

3 | CIRCUIT DESIGN AND MODELING

In previous work, the optical modulation technology described in Section 2 has been successfully applied to demonstrate a variety of tunable/reconfigurable THz circuits/components including modulators/attenuators, coded imaging apertures, and beam steering/forming Fresnel antennas.[18–21] However, tuning and reconfiguring a filter circuit using this technology through the RF switching approach has not yet been fully explored. Although in Li et al.[13] a tunable and reconfigurable BSF prototype based on first-order absorption-mode SRRs has been demonstrated using the proposed optical switching elements, the feasibility and potential of this approach for tuning higher-order more complex BPFs with multiple switching elements have not yet been investigated.

In view of this, to verify the effectiveness of the proposed switching technology for tuning and reconfiguring BPFs, a prototype tunable and reconfigurable BPF was designed as shown in Figure 1B. The BPF implementation features a second-order design with two closely coupled square-loop SRRs operating in transmission mode (in series in a 50 Ω microstrip transmission line configuration). Each SRR has an optical switching element embedded at its gap. In principle, when the switching element is turned off, the SRR operates as a half-wavelength resonator. When the switching element is on, the SRR structure is reconfigured to work as a ring resonator with resonant frequency nearly doubled.[22] By controlling the two switching elements simultaneously (for higher performance), the frequency response of the BPF circuit can be dynamically reconfigured between bandpass and broadband suppression.

Although BPFs employing single transmission-mode SRR using one switching element could be adopted for prototype demonstration (of a tunable BPF),[23] the design in Figure 1B with two SRRs allows us to fully reveal the potential and design flexibility of the proposed approach while achieving a higher filter performance (e.g., higher roll-off). In addition, the design involves electric coupling between two SRRs with two gaps closely located facing each other (with a small distance D).[14] It would be quite challenging for tuning the two SRRs simultaneously using any other switching technology requiring complex biasing circuit. This will again allow us to demonstrate the unique advantage of the proposed approach using spatially resolved optical tuning and modulation with a spatial resolution primarily determined by the light wavelength.[16,17] It is worth to point out that once tunable BSFs using absorption-mode SRRs and BPFs using transmission-mode SRRs are demonstrated, more advanced microwave filters with arbitrary frequency responses and multiple functionalities (e.g., dual-band BPFs) can be designed using combinations of the two modes.

Based on the above analysis, the proposed BPF circuit (see Figure 1B) was designed on a RO5880 substrate (with dielectric constant of 2.2, thickness of 0.51 mm, copper thickness of 0.035 mm, and loss tangent of 0.001). For a prototype demonstration, the center frequency of the passband was chosen to be 3 GHz. To achieve the desired 3 GHz target frequency, the side length (L) of the square-loop SRR was calculated as 11 mm. The width (W) of the microstrip is set at 1.5 mm, same as the main line width for a 50 Ω characteristic impedance in the 2–4 GHz frequency range. Furthermore, to ensure a uniform width of 1.5 mm, the corner section of the square-loop SRRs was intentionally removed. This particular dimension was designed for reducing the mismatch between SRRs and the input/output transmission line. The distance (D) between the two adjacent SRRs was designed to be 0.3 mm for efficient electric coupling while facilitating easy fabrication. The gap size (G) for each SRR is of 0.4 mm (roughly the size of the light spot from the optical fiber employed). For simulation, it is assumed that a 73 μm thick silicon thin film (used in our previous demonstration) with an area of $1 \times 2\ mm^2$ is positioned over the gap region of each SRR, ensuring good contact between the Si and SRR strip lines (see Figure 1C).

To explore the best performance that can be achieved using this approach, the carrier concentration and photoconductivity of the Si active layer were calculated using the physics-based model in[11] assuming an incident light intensity of $100\ W/cm^2$ (based on Figure 2). The resulting material parameters were then used in ADS simulation. Figure 3 illustrates the simulation results of the proposed BPF. When both the switching elements are in the off-state (no light illumination), the circuit shows a passband centered at 3.01 GHz which is slightly higher than the designed value. The 3-dB bandwidth is 250 MHz, or 8.3%. The average insertion loss (IL, S_{21}) in the passband is approximately 0.7 dB, with a return loss (RL, S_{11}) reaches a level of ~40 dB at the center frequency of 3.01 GHz. Owing to the adoption of second-order two-SRR design, the BPF shows high roll-off with a sharp transition from the passband to stopband. The null suppression is 56.7 and 51.4 dB at 2.55 and 3.72 GHz,

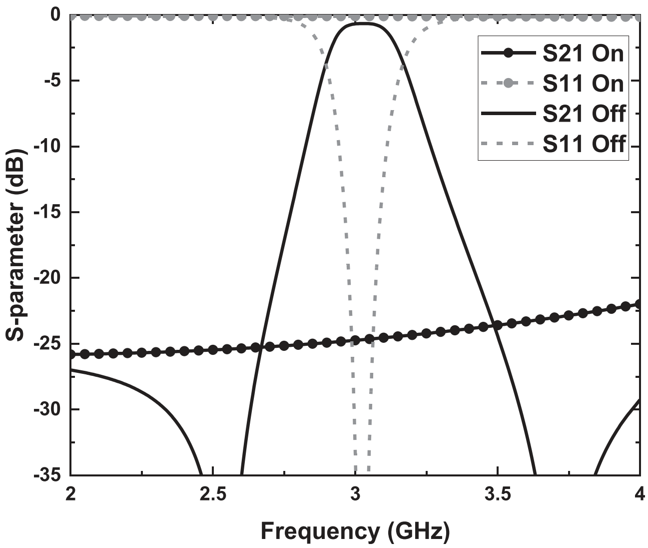

FIGURE 3 Simulated S-parameters of the proposed bandpass filter for the on-state and off-state assuming a switching light intensity of 100 W/cm^2.

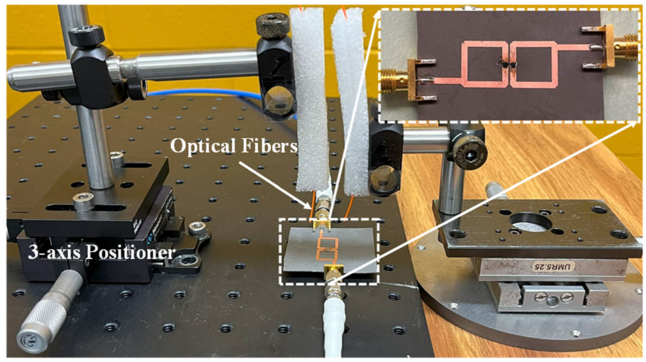

FIGURE 4 Photograph of the implemented bandpass filter (BPF) circuit and experiment set-up. Inset: the prototype BPF with implemented silicon on the top of the gap.

respectively. The stopband ripple level is beyond 25 dB. Although the above BPF parameters can be adjusted or further improved (e.g., extremely narrow bandwidth bandpass/stop filter) by modifying the circuit geometry,[24] in this paper, we focus on the tuning and reconfiguring of the filter using optical modulation. As shown in Figure 3, when the two switching elements are in the on-state (with 100 W/cm^2 illumination using a laser diode), the bandpass response can be dynamically reconfigured to a broadband suppression as expected. The suppression in the original passband achieves ~25 dB (as compared to 0.7 dB), while the reflection coefficient S_{11}, remains low at ~0.1 dB over the entire frequency range spanning from 2 to 4 GHz. These results indicate the successful realization of a reconfigurable bandpass filter by employing the proposed optically controlled switching technology.

4 | BPF CIRCUIT IMPLEMENTATION AND MEASUREMENT

The designed BPF circuit was fabricated on a RO5880 substrate using a conventional photolithography process (photoresist MICROPOSIT S1813) followed by ferro chloride acid etching. Two SMA connectors (Amphenol RF 132255-11) were used at the input and output ports for S-parameter measurement. To enable the BPF tuning and reconfiguring as simulated in Section 3, two micromachined Si chips with a thickness of 73 μm and a dimension of ~1 × 2 mm^2 were manufactured using a deep reactive-ion etching (DRIE) process and were then attached (glued using silver epoxy) on top of the gaps in each SRR as shown in Figure 4 inset. For light illumination, two laser diodes (QSP-808-4 model) from Qphotonics LLC, were subjected to variable biasing currents to modulate their output light intensities. The emitted light from the diodes was channeled through two optical fibers (with a diameter ~300 μm) and directed to illuminate the two silicon chips respectively, at normal incidence, as illustrated in Figure 4. The distance between the fiber tips and the silicon chips was consistently maintained at ~1 mm for prototype demonstration. The laser diode employed possess a maximal output power of 4 W when operated under a biasing current of 5 A. For the purpose of the prototype demonstration described in this work, two Agilent E3610A DC power supplies, were employed. These power supplies are capable of delivering a maximum current of 3 A, corresponding to an approximate power output of ~2 W. To achieve precise control over the illumination characteristics, the positioning and elevation of the fiber tips were adjusted. This adjustment was facilitated by employing Thorlabs three-axis micro-positioners, which offer submicron resolution. Consequently, a light spot with an approximate diameter of 1.0 mm^2 was generated on each silicon chip, resulting in an estimated maximum effective light intensity of ~40 W/cm^2 for 3 A biasing current. This estimation takes into account the light reflection and absorption coefficient of the silicon active layer. In addition, in this prototype demonstration, the thickness of the Si active layer employed has a thickness of ~73 μm which is significantly larger than the 41.6 μm calculated diffusion length, leading to exponentially decreased carrier concentration along the light incident direction (normal to the Si surface).[16] As a result, the achievable

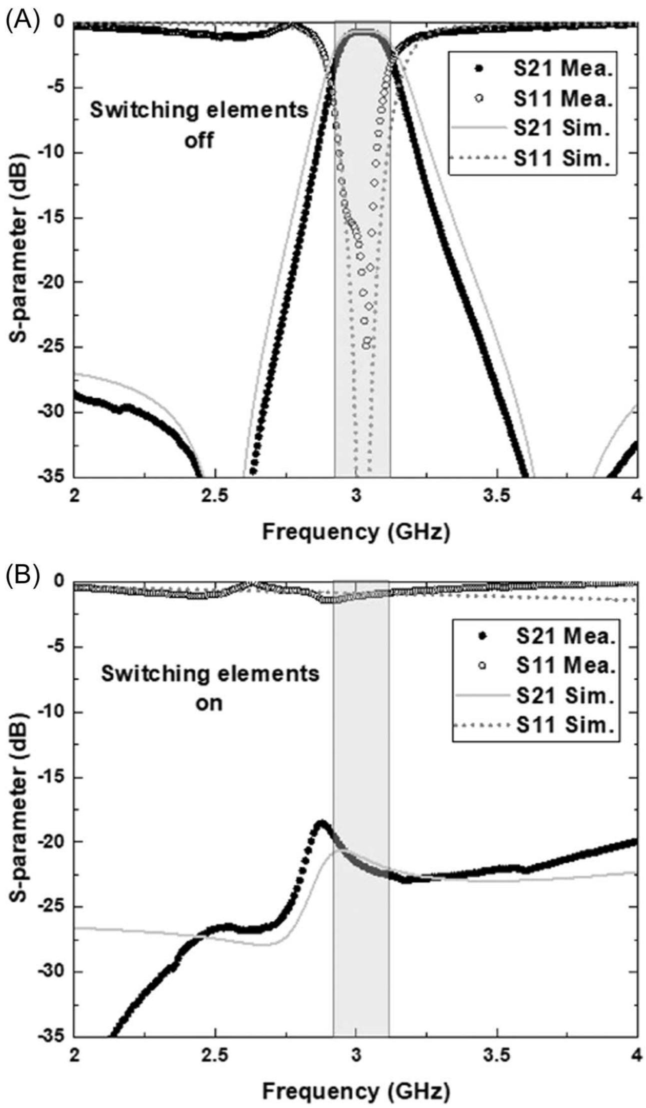

FIGURE 5 The simulated and measured frequency response of the bandpass filter in (A) off-state and (B) on-state, and 3 dB passband is highlighted as a shadow region.

photoconductivity near the bottom surface of the Si is equivalent to a value due to a much lower light intensity (which is ~40 W/cm^2). According to Figure 2, a much thinner Si chip can be used for improved performance. By changing the biasing currents of the two laser diodes simultaneously from 0 to 3 A, the active regions of the two Si switching elements are illuminated with different effective light intensities for tuning/reconfiguring. On the basis of previous stability testing of the proposed photoconductivity approach, we expect that the switches will demonstrate sufficient stability for applications at room temperature.[18] The S-parameters of the BPF circuit in the frequency range of 2.0–4.0 GHz were then measured using a Keysight network analyzer (E5080B).

5 | MEASUREMENT RESULTS

Figure 5 shows the measured and corresponding simulated frequency responses for the proposed BPF prototype when the switching elements are in the off- and on-states. As shown in Figure 5A, when the two laser diodes are turned off (off-state), the proposed BPF shows a single passband filtering response as expected. The measured center frequency is located at 3.03 GHz, and the 3-dB bandwidth is 200 MHz (i.e., 6.7%). The slightly smaller measured 3-dB bandwidth and the higher measured center frequency, when compared with simulation, may be attributed to the imperfect circuit fabrication. At the center frequency (i.e., 3.03 GHz), the measured insertion loss (S_{21}) is ~0.75 dB, while the reflection coefficient S_{11} reaches ~25 dB. In addition, owing to the employment of higher-order two SRR design, the measured BPF response indeed shows higher roll-off characteristics[23] with a measured null suppression of 63.7 dB at 2.55 GHz, and 48.4 dB at 3.73 GHz. The measured stopband ripple level exceeds 25 dB. Overall, the measured results agree quite well with the design and simulation.

As shown in Figure 5B, when the two laser diodes are turned on (or on-state) simultaneously using the maximum biasing current, that is, 3A (with an estimated light intensity of ~40 W/cm^2), the BPF response can be successfully reconfigured to a broadband suppression response. The S_{21} of the circuit is suppressed to be generally lower than ~−18.5 dB, and the S_{11} remains higher than ~−1 dB across the entire frequency range from 2 to 4 GHz. Specifically at 3.03 GHz (center frequency of the BPF response), the suppression is ~22 dB, reconfigured from a pass response (S_{21} in Figure 5A) of ~0.75 dB, showing strong reconfigurability as designed. These results generally align very well with the simulation results obtained using the estimated power intensity of 40 W/cm^2 and a lifetime $\tau = 1\,\mu$s (verified) as shown in Figure 5B, demonstrating the effectiveness of the BPF design/modeling using the physics-based model. As compared to the simulated best performance using a light intensity of 100 W/cm^2 in Figure 3, the suppression level in the original passband (see shadow region in Figure 5) for the on-state is only slightly lower (compared to an average of 25 dB), indicating that by employing a modified, thinner silicon chip and increasing the incident light intensity, a significantly high photoconductivity can be achieved for realizing high-performance switches with low insertion loss (or attenuation).

In addition to reconfiguring the BPF response between the two states (on and off), the reported approach of optical modulation offers a unique

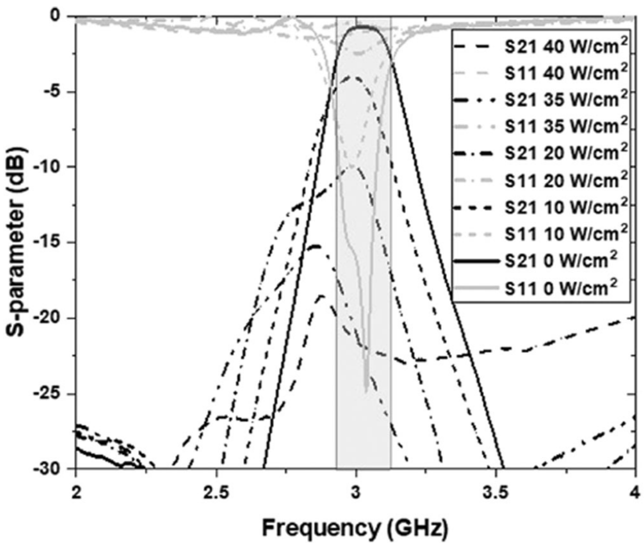

FIGURE 6 The frequency response of the bandpass filter with the switching elements illuminated using different light intensities. The 3 dB passband is highlighted as a shadow region.

opportunity for continuously tuning the passband attenuation/suppression. To demonstrate this unique feature of the proposed technology, the intensities of the illumination light from the two laser diodes were adjusted by continuously changing the biasing currents from 0 to 3 A simultaneously. Figure 6 illustrates the measured S-parameter for selected different light intensities (i.e., 0, 10, 20, 35, and 40 W/cm^2) estimated using the physics-based model (with $\tau = 1\ \mu s$) described earlier. As can be seen, the center frequency attenuation level (S_{21}) exhibits a continuous shift from 0.75 to ~22 dB, while the S_{11} decreased from 25 to ~1 dB, as the light intensity is incremented from 0 to 40 W/cm^2. The estimated power levels based on modeling agree well with the calculation using the power-current data sheet provided by the laser diode manufacturer (Qphotonics, LLC). This unique feature of continuous tuning the passband attenuation (of BPFs) may enable the development of more advanced circuit functionalities for next-generation communication systems.[25]

6 | DISCUSSION

Although strong tuning and reconfiguring capability for a prototype BPF using the proposed optical modulation approach has been successfully demonstrated, the results presented above also suggest that the switching element on/off ratio and the resulting BPF tuning performance can be further improved. Figure 2 shows the photoconductivity achieved and used in this work as compared to modeling for illustrating the great potential. First, as seen in Figure 2, increasing the light intensity can generate a greater number of electron-hole pairs, thus enhancing carrier concentration and substantially improving achievable photoconductivity. Second, using a thinner silicon for active layer not only increases photoconductivity (as demonstrated in Figure 2, or reduces power for same photoconductivity) but also prevents a significant drop in carrier concentration due to the relatively short diffusion length (e.g., 41.6 μm compared to the 73 μm Si thickness in this paper). In addition, switching elements using Ge as the active layer can be employed for even higher achievable photoconductivity since Ge offers a higher carrier lifetime (i.e., 1 ms) and light absorption coefficient (i.e., $5.03 \times 10^5\ cm^{-1}$) when compared to Si (with only 1 μs and $6.7 \times 10^3\ cm^{-1}$, respectively). Finally, fully integrated switching elements using a noncontact configuration for eliminating the rapid carrier recombination at the contacts as described in Shi et al.,[11] and Li et al.[12] can be adopted for optimized both device and filter performance. The power consumption of the proposed switching approach could be significantly reduced by integrating ferroelectric (FE) latching for nonvolatile operation.[12,26]

Another key consideration for dynamically tuning and reconfiguring BPFs is the operation speed. The operation speed of the proposed BPF is primarily determined by the carrier lifetime inside the active layer (i.e., Si or Ge) of the switching elements employed. This lifetime depends on a number of factors, including the surface and bulk defect density in the silicon, substrate thickness and geometry, as well as the photo-induced carrier density. In this prototype demonstration, the Si wafer used has a relatively short lifetime ($\tau = \sim 1\ \mu s$) estimated from our previous work.[16–19] The 3 dB operation bandwidth of the tunable and reconfigurable BPF demonstrated was estimated to be ~200 kHz (using $f_{3\,dB} = 1/[2\pi\tau]$). A much higher switching speed of 2 MHz has been measured using Si with even shorter lifetime,[27] indicating the potential for achieving high-speed dynamic tuning and reconfiguring. However, a short lifetime unavoidably leads to lower achievable carrier concentration and hence photoconductivity, therefore a trade-off between switching speed and performance has to be made for designing such tunable/reconfigurable BPFs using the proposed optical modulation approach.

Of particular importance, it is seen from the demonstration (i.e., tuning two closely located switching elements simultaneously without biasing circuitry) that the proposed optical modulation technology offers a significant advantage in terms of universal adaptability, as it eliminates the need for biasing circuits. This key feature greatly increases the flexibility in circuit (e.g., BPFs) design, fabrication, and integration, especially for the circuits operating within the high-frequency spectrum. As a result, the proposed filter design can be easily scaled up for mmW-THz operation without extensive structural modifications. In addition, as demonstrated in Shi et al.,[11] and Li et al.[12] THz switches using the proposed mechanism show superior RF performance as compared to most THz switches using different technologies. Finally, it is worth noting that the demonstrated switching approach can exploit spatial optical modulation and operation using computer-programmed light patterns without any extra biasing circuits, making it suitable for large-scale switch array or network applications, enabling the development of more advanced and complex THz/microwave filters (e.g., the filter banks in Figure 1) with a large number of switching elements. The proposed approach for tunable and reconfigurable BPFs may pave the way for developing THz/microwave adaptive circuits for advanced sensing, imaging, and communication applications.[28]

7 | CONCLUSION

In summary, this paper presents a novel approach using photoconductivity modulation in semiconductors for realizing dynamic tuning and reconfiguring BPFs with high performance. For a prototype demonstration, a BPF was designed using two closely coupled SRRs in the transmission mode. Each SRR was embedded with a micromachined Si chip at its gap for switching. Measurement results show that the BPF response can be dynamically reconfigured (between bandpass and broadband suppression) and the in-band attenuation can be continuously tuned. In addition, a much higher tuning/reconfiguring performance can be achieved by using higher light intensity, thinner active layer, or semiconductors with longer lifetime. Most importantly, this approach eliminates the need for biasing circuits, and demonstrates the potential in terms of universal adaptability, design flexibility, and frequency scalability. Consequently, the proposed approach holds great promise for the development of adaptive microwave-to-THz circuits for next-generation advanced sensing, imaging, and communications.

ACKNOWLEDGMENTS

This work was partially supported by the National Science Foundation (NSF) under the grants of ECCS-1711052, ECCS-1711631, and ECCS-2223949.

DATA AVAILABILITY STATEMENT

The data that support the findings of this study are available from the corresponding author upon reasonable request.

ORCID

Yijing Deng http://orcid.org/0000-0003-3352-8867

REFERENCES

1. Simpson DJ, Gomez-Garcia R, Psychogiou D. Single-/multi-band bandpass filters and duplexers with fully reconfigurable transfer-function characteristics. *IEEE Trans Microw Theory Tech*. 2019;67(5):1854-1869.
2. Chi PL, Yang T, Tsai TY. A fully tunable two-pole bandpass filter. *IEEE Microw Wirel Comp Lett*. 2015;25(5):292-294.
3. Won-Yeol lee L, Akyildiz IF. Optimal spectrum sensing framework for cognitive radio networks. *IEEE Trans Wirel Commun*. 2008;7(10):3845-3857.
4. Crespin ER, Olsson RH, Wojciechowski KE, et al. Fully integrated switchable filter banks. *IEEE/MTT-S International Microwave Symposium Digest*, Montreal, QC, Canada, 2012, pp. 1-3.
5. Parke J, Freitag R, Torpey M, et al. High-performance SLCFETs for switched filter applications. *IEEE Compound Semiconductor Integrated Circuit Symposium (CSICS)*, Austin, TX, USA, 2016, pp. 1-4.
6. Gentili F, Urbani L, Bianchi G, Pelliccia L, Sorrentino R. p-I-n-diode-based four-channel switched filter bank with low-power TTL-compatible driver. *IEEE Trans Microw Theory Tech*. 2014;62(12):3333-3340.
7. Guyette AC. Intrinsically switched varactor-tuned filters and filter banks. *IEEE Trans Microw Theory Tech*. 2012;60(4): 1044-1056.
8. Reines IC, Goldsmith CL, Nordquist CD, et al. A low loss RF MEMS Ku-band integrated switched filter bank. *IEEE Microw Wirel Comp Lett*. 2005;15(2):74-76.
9. Albina CM, Hackl G. Layout parasitic interconnections effects on high frequency circuits, *6th IEEE Dallas Circuits and Systems Workshop on System-on-Chip*, 2007, pp. 1-4.
10. Grant PD, Denhoff MW, Mansour RR. A comparison between RF MEMS switches and semiconductor switches, *International Conference on MEMS, NANO and Smart Systems (ICMENS'04)*, 2004, pp. 515-521.
11. Shi Y, Deng Y, Ren J, Li P, Fay P, Liu L. Computational analysis of novel high performance optically controlled RF switches for reconfigurable millimeterwave-to-THz circuits. *OSA Contin*. 2021;4:2642-2654.
12. Li P, Wu W, Shi Y, Deng Y, Fay P, Liu L. Broadband THz switching with extremely low insertion loss and superior isolation, *IEEE/MTT-S International Microwave Symposium - IMS* 2023, 2023, pp. 688-691.
13. Li P, Shi Y, Deng Y, Fay P, Liu L. Tunable and reconfigurable bandstop filters enabled by optically controlled RF switching elements. *Electron Lett*. 2022;58(25):985-987.
14. Hong JS, Lancaster MJ. Couplings of microstrip square open-loop resonators for cross-coupled planar microwave filters. *IEEE Trans Microw Theory Tech*. 1996;44(11):2099-2109.
15. Arora ND, Hauser JR, Roulston DJ. Electron and hole mobilities in silicon as a function of concentration and temperature. *IEEE Trans Electron Devices*. 1982;29(2): 292-295.
16. Kannegulla A, Shams MIB, Liu L, Cheng LJ. Photo-induced spatial modulation of THz waves: opportunities and limitations. *Opt Express*. 2015;23:32098-32112.

17. Cheng LJ, Liu L. Optical modulation of continuous terahertz waves towards cost-effective reconfigurable quasi-optical terahertz components. *Opt Express*. 2013;21:28657-28667.
18. Ren J, Jiang Z, Fay P, Hesler JL, Tong CYE, Liu L. High-performance WR-4.3 optically controlled variable attenuator with 60-dB range. *IEEE Microw Wirel Comp Lett*. 2018;28(6): 512-514.
19. Jiang Z, Shams MIB, Cheng LJ. Investigation and demonstration of a WR-4.3 optically controlled waveguide attenuator. *IEEE Trans Terahertz Sci Technol*. 2017;7(1):20-26.
20. Shams MIB, Jiang Z, Rahman SM, et al. A 740-GHz dynamic two-dimensional beam-steering and forming antenna based on photo-induced reconfigurable Fresnel zone plates. *IEEE Trans Terahertz Sci Technol*. 2017;7(3):310-319.
21. Deng Y, Shi Y, Li P, Fay P, Cheng LJ, Liu L. A cost-effective approach for achieving subwavelength THz imaging using photoinduced coded-apertures on mesa-array structures. *IEEE Trans Terahertz Sci Technol*. 2022;12(6):658-666.
22. Bernard PA, Gautray JM. Measurement of dielectric constant using a microstrip ring resonator. *IEEE Trans Microw Theory Tech*. 1991;39(3):592-595.
23. Syahral M, Munir A. Development of multiple elements of SRR-based Bandpass Filter, *10th International Conference on Telecommunication Systems Services and Applications (TSSA)*, 2016, pp. 1-4.
24. Lin XQ, Cui TJ. Controlling the bandwidth of split ring resonators. *IEEE Microw Wirel Comp Lett*. 2008;18(4):245-247.
25. Dogan H, Meyer RG. Intermodulation distortion in CMOS attenuators and switches. *IEEE J Solid State Circ*. 2007;42(3): 529-539.
26. Khan AI, Keshavarzi A, Datta S. The future of ferroelectric field-effect transistor technology. *Nat Electron*. 2020;3:588-597.
27. Connors JA, Tong CYE, Grimes PK, Gebreyohannes A, Liu L. Measurement and design of a waveguide probe based WR 3.4 optically controlled modulator, *28th International Symposium on Space Terahertz Technology*, University of Cologne, 2017.
28. Berceli T, Herczfeld PR. Microwave photonics—a historical perspective. *IEEE Trans Microw Theory Tech*. 2010;58(11): 2992-3000.

How to cite this article: Li P, Zahedi E, Shi Y, Deng Y, Liu L. Dynamically tuning and reconfiguring microwave bandpass filters using optical control of switching elements. *Microw Opt Technol Lett*. 2024;66:e34082. doi:10.1002/mop.34082